The HIF target ATG9A is essential for epithelial barrier function and tight junction biogenesis

Alexander S. Dowdell[a], Ian M. Cartwright[a], Matthew S. Goldberg[a], Rachael Kostelecky[a], Tyler Ross[a], Nichole Welch[a], Louis E. Glover[a,b], and Sean P. Colgan[a,*]

[a]Mucosal Inflammation Program and Division of Gastroenterology and Hepatology, University of Colorado, Aurora, CO 80045; [b]School of Biochemistry and Immunology, Trinity College Dublin, D2, D02 PN40, Ireland

ABSTRACT **Intestinal epithelial cells (IECs) exist in a metabolic state of low oxygen tension termed "physiologic hypoxia." An important factor in maintaining intestinal homeostasis is the transcription factor hypoxia-inducible factor (HIF), which is stabilized under hypoxic conditions and mediates IEC homeostatic responses to low oxygen tension. To identify HIF transcriptional targets in IEC, chromatin immunoprecipitation (ChIP) was performed in Caco-2 IECs using HIF-1α- or HIF-2α-specific antibodies. ChIP-enriched DNA was hybridized to a custom promoter microarray (termed ChIP-chip). This unbiased approach identified autophagy as a major HIF-1-targeted pathway in IEC. Binding of HIF-1 to the ATG9A promoter, the only transmembrane component within the autophagy pathway, was particularly enriched by exposure of IEC to hypoxia. Validation of this ChIP-chip revealed prominent induction of ATG9A, and luciferase promoter assays identified a functional hypoxia response element upstream of the TSS. Hypoxia-mediated induction of ATG9A was lost in cells lacking HIF-1. Strikingly, we found that lentiviral-mediated knockdown (KD) of ATG9A in IECs prevents epithelial barrier formation by >95% and results in significant mislocalization of multiple tight junction (TJ) proteins. Extensions of these findings showed that ATG9A KD cells have intrinsic abnormalities in the actin cytoskeleton, including mislocalization of the TJ binding protein vasodilator-stimulated phosphoprotein. These results implicate ATG9A as essential for multiple steps of epithelial TJ biogenesis and actin cytoskeletal regulation. Our findings have novel applicability for disorders that involve a compromised epithelial barrier and suggest that targeting ATG9A may be a rational strategy for future therapeutic intervention.**

Monitoring Editor
Alpha Yap
University of Queensland

Received: May 6, 2020
Revised: Jul 17, 2020
Accepted: Jul 24, 2020

This article was published online ahead of print in MBoC in Press (http://www.molbiolcell.org/cgi/doi/10.1091/mbc.E20-05-0291) on July 29, 2020.

Competing interests: The authors declare that no conflicts of interest exist.

Author contributions: A.S.D. developed experimental design, executed experiments, analyzed data and wrote manuscript; I.M.C., M.S.G., R.K., T.R., and N.W. executed experiments; L.E.G. developed experimental design and executed experiments; S.P.C. advised experimental design, wrote and edited the manuscript.

*Address correspondence to: Sean P. Colgan (sean.colgan@cuanschutz.edu).

Abbreviations used: BafA1, bafilomycin A1; BCS, bovine calf serum; BSA, bovine serum albumin; ChIP-chipchromatin immunoprecipitation-enriched DNA hybridized to a custom promoter microarray; CTD, chromatin immunoprecipitation-enriched DNA hybridized to a custom promoter microarray; CTDcytoplasmic domain; FITC, fluorescein isothiocyanate; HBSS, Hank's balanced salt solution; HIF, hypoxia-inducible factor; HRE, hypoxia response element; IBD, inflammatory bowel disease; IEC, Intestinal epithelial cell; KD, knockdown; MEME, de novo motif; ROS, reactive oxygen species; TBS, Tris-buffered saline; TEER, transepithelial electrical resistance; TJ, tight junction; TSS, transcription start site.

INTRODUCTION

The inflammatory bowel diseases (IBD) are a family of chronic gastrointestinal pathologies, in which a confluence of environmental, genetic, and microbiological risk factors interact to trigger recurrent intestinal inflammation (Baumgart and Carding, 2007). Although the exact etiology of IBD is unknown, polymorphisms in macroautophagy (hereafter referred to as autophagy) genes have been demonstrated to confer susceptibility to the disease (Lassen and Xavier, 2017). Autophagy is an evolutionarily conserved subcellular pathway in which cytoplasmic material is packaged into a distinct, double-membrane vesicle (the "autophagosome") and degraded in the lysosome, after which biomolecules can be salvaged by the cell and recycled (Allen and Baehrecke, 2020). As a pathway, autophagy is constitutively active in the cell but can be further activated by numerous cellular stresses, such as nutrient starvation, oxidative stress, infection by pathogens, and hypoxia (Menikdiwela *et al.*, 2020). The autophagic defense against pathogens, termed "xenophagy," is especially relevant regarding genetic susceptibility to IBD—many autophagy genes identified as IBD risk factors, such as *atg16l1* and

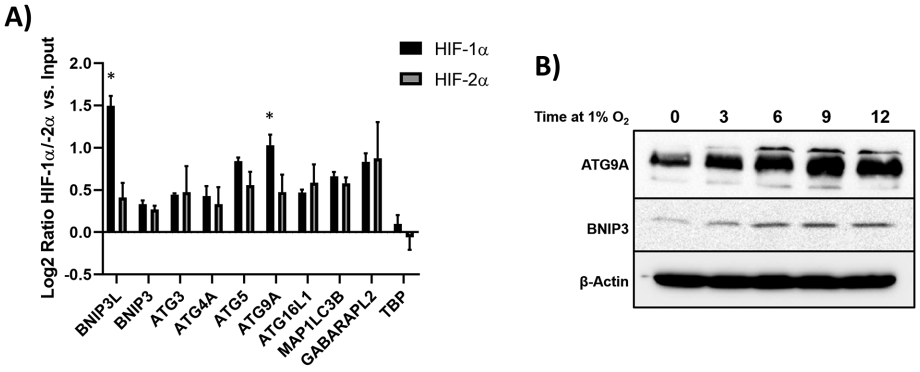

FIGURE 1: Identification of ATG9A as a HIF target gene. (A) ChIP-chip analysis of hypoxia-treated Caco-2 cells demonstrates enrichment of autophagy genes by anti-HIF-1α/-2α pull down vs. input DNA. *$p < 0.05$ by *t* test for HIF-1α vs. HIF-2α pull downs, indicating significantly more binding by HIF-1α for these genes. (B) Hypoxia treatment of T84 cells demonstrates induction of ATG9A by western blot. BNIP3 was used as a positive control for a known hypoxia-regulated gene.

irgm, have been shown to be essential for efficient defense against intracellular bacteria (Abraham and Cho, 2009; Chauhan *et al.*, 2015). Indeed, the very first gene to be identified as an IBD risk factor was *nod2*, the product of which acts as a cytoplasmic peptidoglycan sensor (Hugot *et al.*, 2001; Ogura *et al.*, 2001; Yamamoto and Ma, 2009). The importance of autophagy in IBD is further underscored by clinical observations that autophagy activators improve outcomes in IBD patients, although as of yet, no FDA-approved IBD treatments target this pathway (Massey *et al.*, 2008; Mutalib *et al.*, 2014; Merck, April 2019).

It is notable that the colon exists in a state of "physiologic hypoxia" (Karhausen *et al.*, 2004) where luminal oxygen tensions range from 30 mm Hg in the duodenum to <3 mm Hg in the sigmoid colon (He *et al.*, 1999; Taylor and Colgan, 2017). In such an austere environment, intestinal epithelial cells (IECs) adapt to low oxygen tensions through the transcription factor family hypoxia-inducible factor (HIF), which acts to orchestrate the cellular response to hypoxia through regulation of a specific subset of genes (Glover and Colgan, 2017). The HIF transcription factor family is comprised of three cytoplasmic, oxygen-labile subunits (HIF-1α/-2α), which heterodimerize with a nuclear, oxygen-insensitive subunit (HIF-1β or ARNT) (Lendahl *et al.*, 2009). Low oxygen tensions inhibit the enzymes that label HIF-α for degradation, leading to its cytoplasmic accumulation, nuclear translocation, and dimerization with HIF-1β. The HIF-α/β dimer then binds specific DNA regions, termed hypoxia-response elements (HREs), to modulate gene transcription in response to low oxygen (Lendahl *et al.*, 2009).

Both HIF-1 and HIF-2 are stabilized in inflamed mucosa from human IBD patients (Giatromanolaki *et al.*, 2003) and in mouse models of colitis (Karhausen *et al.*, 2004). Studies of murine IBD have revealed that loss of epithelial HIF-1 correlates with more severe clinical symptoms, while constitutive activation of HIF-1 is protective (Karhausen *et al.*, 2004). Despite this, the molecular targets of HIF stabilization in IECs are not well characterized. To delineate HIF–1- and HIF–2-specific target loci, we performed ChIP-chip (chromatin immunoprecipitation-enriched DNA hybridized to a custom promoter microarray) analysis of chromatin isolated from hypoxic IECs. This analysis revealed identified autophagy genes as major HIF-1 targets and ATG9A as particularly enriched with HIF-1 ChIP. Surprisingly, we find that ATG9A deficiency in model IEC uncouples the actin cytoskeleton and abolishes barrier function as a result of mislocalization of tight junction (TJ) proteins to the cytoplasm. Our findings demonstrate that ATG9A provides a novel role for ATG9A in TJ biogenesis, epithelial barrier maintenance, and actin cytoskeletal development.

RESULTS

HIF ChIP-chip analysis identifies IEC genes involved in autophagy

To identify HIF transcriptional targets, ChIP was performed in Caco-2 IECs using HIF–1α- or HIF–2α-specific polyclonal antibodies (Figure 1A). ChIP-enriched and input DNA were hybridized to a custom microarray comprising a genomewide set of predicted transcription start site (TSS) flanking sequences at 50-bp resolution (Hartzell *et al.*, 2009). Consistent with previous reports (Hu *et al.*, 2003; Schodel *et al.*, 2011), positive hits included cohorts enriched for both HIF-1 and HIF-2 binding (Kelly *et al.*, 2013). Bioinformatic analyses of corresponding genomic regions for de novo motifs (MEME) and transcription factor binding sites (Cartharius *et al.*, 2005) identified the canonical HRE motif 5′-RCGTG-3′ as a highly represented consensus sequence.

As shown in Figure 1A, several autophagy-associated genes demonstrated considerable enrichment versus input DNA, including *bnip3, bnip3l/nix, atg5, atg16l1, atg3,* and *map1lc3b*. By contrast, the housekeeping gene *tbp* showed little enrichment in immunoprecipitated DNA versus input. Gene ontology analysis of the ChIP-chip hits for HIF-1 revealed an increased fold enrichment for the autophagy biological pathway (GO:0010506, fold enrichment = 1.20, $p < 0.025$); pathways similarly overrepresented were "cellular response to hypoxia" (GO:0071456, fold enrichment = 1.27, $p < 0.025$) and "regulation of angiogenesis" (GO:0045675, fold enrichment = 1.24, $p < 0.01$) (Mi *et al.*, 2019). Interestingly, the autophagy protein *atg9a* was highly enriched in IEC immunoprecipitated samples versus input, with higher enrichment in the HIF-1α precipitated sample. ATG9A is a multi-pass transmembrane protein that is essential for autophagy, as its loss has been shown in numerous studies to inhibit autophagosome formation (Yamada *et al.*, 2005; Saitoh *et al.*, 2009; Imai *et al.*, 2016). In addition, ATG9A has been shown to be essential in vivo, as mice lacking ATG9A die within 1 day of birth (Saitoh *et al.*, 2009). Other studies have shown that ATG9A is regulated by hypoxia in glioblastoma cells and undergoes post-translational regulation during hypoxia in an AMPK-dependent manner to increase autophagic flux (Weerasekara *et al.*, 2014; Abdul Rahim *et al.*, 2017).

ATG9A is induced in hypoxic IECs in a HIF–1-dependent manner

Given the magnitude of ATG9A enrichment by ChIP, we explored the novel regulation of ATG9A by hypoxia in IECs. First, we sought to validate our observation that ATG9A is regulated by HIF/hypoxia in IECs. For our model cell line, we chose to use the colorectal adenocarcinoma cell line T84 versus Caco-2 due to its superiority as a model for the colonic epithelium and its demonstrated history as a system for studying intestinal barrier function (Kelly *et al.*, 2013; Saeedi *et al.*, 2015; Devriese *et al.*, 2017). As shown in Figure 1B, western blot analyses revealed that ATG9A levels were significantly increased by hypoxia in a time-dependent manner.

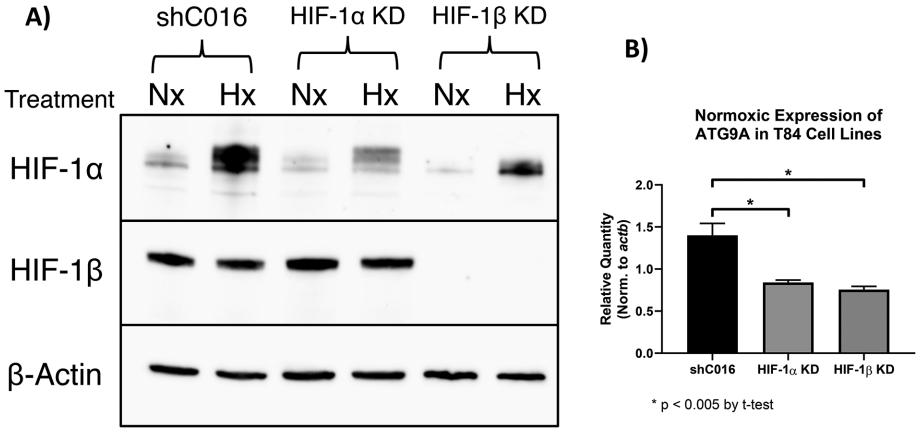

FIGURE 2: KD of HIF-1 impairs induction of ATG9A by Hypoxia. (A) Validation of HIF KD T84 cell lines by western blot. Cells were treated with hypoxia (1% O_2) for 24 h or left untreated at normoxia. See also *Materials and Methods*. (B) Analysis of *atg9a* expression in either control or HIF-1 KD cells by qPCR, normalized to *actb*. The representative experiment shown is of $n = 3$. Statistical significance was calculated by *t* test.

Next, we sought to determine if hypoxic regulation of ATG9A required HIF. To accomplish this, we stably knocked down either HIF-1α or the heterodimeric binding partner HIF-1β in T84 cells using lentiviral shRNA (Figure 2A), as we have done previously (Kelly *et al.*, 2013; Saeedi *et al.*, 2015; Devriese *et al.*, 2017; Zheng *et al.*, 2017). These T84 IECs were then exposed to hypoxia (4 or 20 h), and ATG9A mRNA levels relative to normoxic controls were assessed. As shown in Figure 2B, loss of HIF-1α or HIF-1β resulted in significantly reduced expression of *atg9a* (>40% decrease, $p < 0.005$), demonstrating the dependency of ATG9A induction on functional HIF-1.

As an extension of these results, we examined the *atg9a* promoter sequence for potential HRE motifs (5′-A/GCGTG-3′). To do so, we performed site-directed mutagenesis and functional analysis of ~1 kB of the *atg9a* promoter. Using the JASPAR (Fornes *et al.*, 2020), we identified two putative HRE elements in the wild-type *atg9a* promoter region as shown in Figure 3A. We then mutated the conserved core 5′-CGTG-3′ sequence in each element, exchanging each base with its cognate purine/pyrimidine to a final sequence of 5′-TACA-3′. The final luciferase construct with mutated HREs (pASD3) is shown in Figure 3A, which shows the altered bases in context with the wild-type sequences. These two plasmids were then purified and transfected into HeLa cells, which were used as opposed to Caco-2/T84s cells due to their amenability to transfection and rapid transcriptional/translational responses. Transfected cells were incubated under normoxia or hypoxia conditions for 24 h, and cells were lysed and analyzed for luciferase activity. As depicted in Figure 3B, mutation of the HRE consensus sequences from the *atg9a* promoter decreases the hypoxia-mediated increase in luciferase activity from the normoxic baseline from ~70% to ~30%. It is notable that the HRE mutations did not result in a complete loss of ATG9A induction at hypoxia, suggesting that other HIF-independent pro-autophagy pathways (e.g., AMPK activation, ER stress) may contribute to induction of ATG9A expression in hypoxia (Daskalaki *et al.*, 2018). These data, taken together, demonstrate that ATG9A is regulated, at least in part, by HIF in hypoxia.

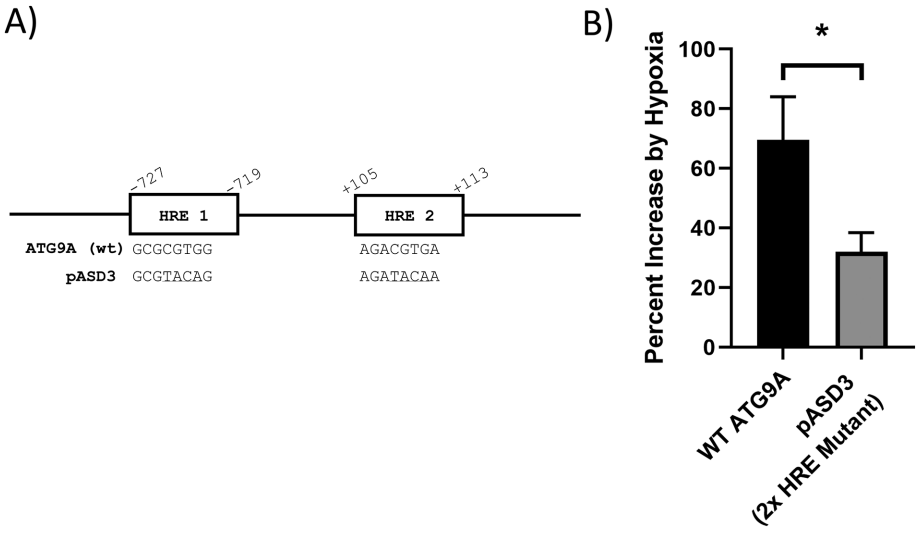

FIGURE 3: ATG9A promoter contains functional HREs. (A) Map of predicted HREs in *atg9a* promoter identified using JASPAR. Numbers correspond to position from ATG9A mRNA transcriptional start site. Underlined regions in pASD3 sequence are mutations made to eliminate putative HREs. (B) Transfection of HeLa cells with LightSwitch plasmid containing either wild-type or mutated (pASD3) ATG9A promoter regions, followed by incubation at either normoxia or hypoxia, demonstrates reduction of hypoxia-induced gene expression following loss of HREs. Data are expressed as the percentage increase of luciferase signal at hypoxia vs. normoxia for a given reporter construct.

ATG9A controls barrier formation in IEC

In IEC, a number of HIF target genes have been shown to contribute to the establishment and maintenance of the epithelial barrier (Furuta *et al.*, 2001; Wartenberg *et al.*, 2003; Louis *et al.*, 2006; Kelly *et al.*, 2013; Saeedi *et al.*, 2015). Therefore, we surmised that ATG9A, as a HIF-regulated gene, may play a role in the regulation of intestinal epithelial barrier. To this end, we generated stable ATG9A knockdowns (KDs) in T84 cells (T84-shATG9A, "ATG9A KD") through lentiviral transduction of shRNA. We also generated T84s transduced with nontargeting shRNA control (T84-shC016, "vector controls"). As shown in Figure 4A, ATG9A was decreased by >90% in the T84 KD cells as compared with vector controls. Resultant cells were grossly normal in appearance, passaged normal, and proliferated similar to control cells. We then assessed epithelial barrier integrity through measurement of transepithelial electrical resistance (TEER), a standard assay for the quantitation of epithelial barrier strength, in both the controls and the ATG9A KD cells (Furuta *et al.*, 2001; Kelly *et al.*, 2013, 2015; Zheng *et al.*, 2017).

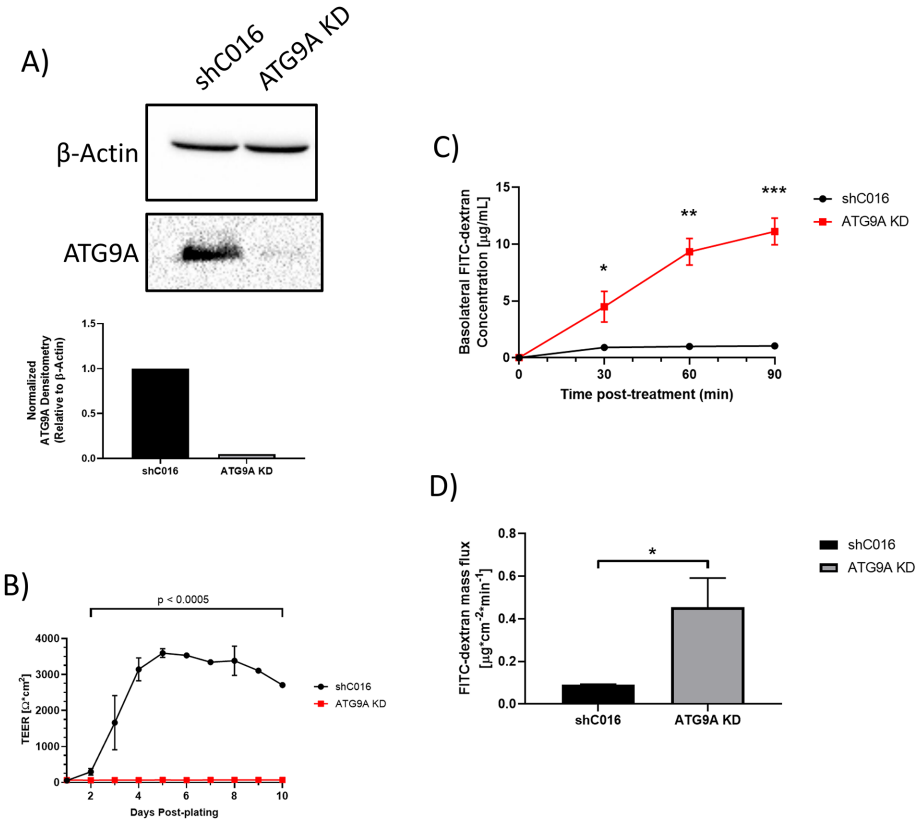

FIGURE 4: Loss of ATG9A negatively impacts barrier function in IECs. (A) T84 control or ATG9A-depleted cells were analyzed for ATG9A expression by western blotting, shown with a representative blot. Quantification of ATG9A decrease was performed using ACTB-normalized densitometry. (B) T84-shC016 or T84 ATG9A KD cells were plated on transwell inserts as described in *Materials and Methods,* and TEERs were measured daily. (C) T84-shC016 or T84 ATG9A KD cells plated on inserts were treated with 4 kDa FITC-dextran on the apical side. Fluorescence was measured from buffer aliquots taken from the basolateral chamber every 30 min. (D) Analysis of FITC-dextran mass flux was calculated at the $t = 30$-min time point using measurements from Figure 3C. All statistics calculated using *t* test.

As depicted in Figure 4B, loss of ATG9A nearly completely abolishes barrier formation (not exceeding 100 Ω*cm^2), whereas vector control cells demonstrated considerable barrier formation over time (greater than 3000 Ω*cm^2). In addition, this barrier defect could not be restored through treatment with sodium butyrate, a known pro-barrier factor (Kelly *et al.*, 2015; Zheng *et al.*, 2017; Wang *et al.*, 2020), indicating that the barrier defect in ATG9A KD cells is likely not due to energetic deficits (Supplemental Figure S1).

To verify barrier dysfunction in ATG9A KD cells, paracellular permeability was assessed. To do this, a fluorescent tracer fluorescein isothiocyanate (FITC)-dextran (4 kDa) was added to the apical chamber of cell monolayers, and passage through TJs was monitored over time. Figure 4, C and D demonstrate that ATG9A KD cells permit a significantly higher rate of FITC-dextran diffusion across the monolayer at >0.4 μg*cm^{-2}*min^{-1}, whereas vector control cells show significant resistance to FITC-dextran permeability at <0.1 μg*cm^{-2}*min^{-1} ($p < 0.0001$ compared with ATG9A KD). These data demonstrate that ATG9A is essential for proper establishment of epithelial barrier.

ATG9A determines AJ, TJ localization in IEC

Given the magnitude of barrier deficiency in ATG9A KD, we next determined whether TJs formed normally in these cells. To accomplish this, we cultured ATG9A KD cells and vector controls on transwell polyester membrane permeable supports and stained methanol-fixed cells for the TJ proteins occludin and ZO-1, as done before (Wang *et al.*, 2016). Our results (Figure 5A) indicate that ZO-1 and occludin are both markedly mislocalized in ATG9A KD cells. Compared to the classic "chicken wire" pattern (Kelly *et al.*, 2013; Saeedi *et al.*, 2015) shown in vector control cells, ATG9A KD cells demonstrated an abnormal cytoplasmic distribution of both occludin and ZO-1 in the majority of cells. Sparse clusters of ATG9A KD cells appeared to show ZO-1/occludin distribution similar to control cells—we ascribe this to the polyclonal nature of the lentivirus transduced cell population. Similarly to TJ components, the adherens junction protein E-cadherin is mislocalized by depletion of ATG9A (Figure 5B). However, biochemical analysis of selected TJ (claudin-1/-2) and adherens junction (E-cadherin) proteins by western blot showed a surprisingly normal pattern (Figure 5C). While claudin-1 levels were diminished by ~50%, claudin-2 and E-cadherin expression was relatively intact. Such findings suggest that the barrier defect associated with the loss of ATG9A is not likely decreased overall expression of TJ proteins. Interestingly, depletion of ATG9A did not influence cell polarization of surface protein as can be seen from staining cell monolayers with antibodies against the apical marker CD55 (Lawrence *et al.*, 2003) (Supplemental Figure S3), suggesting that protein mislocalization may be specific to junctional proteins.

We also sought to examine whether pharmacological inhibition of autophagy could replicate the observed phenotypes in ATG9A-depleted cells. As shown in Supplemental Figure S2, treatment of T84 cells with bafilomycin A1 (BafA1), a well-characterized inhibitor of autophagic flux, inhibits development of epithelial barrier function, in a similar manner as ATG9A depletion. This inhibition was found to be reversible, as a "washout" of the monolayers after 24 h incubation with BafA1 permitted recovery of barrier function over time. Additionally, BafA1 induced dramatic morphological alterations in monolayer AJs and TJs as observed by confocal immunofluorescence. These alterations were reminiscent of those seen in HIF–1β-depleted T84 cells, which demonstrated similar barrier defects and "undulating" TJs (Saeedi *et al.*, 2015). These data demonstrate that inhibition of autophagy as a process is detrimental to the establishment and maintenance of the epithelial barrier.

Depletion of ATG9A induces actin cytoskeletal abnormalities and VASP mislocalization

Given the striking defect in epithelial barrier observed in ATG9A-depleted cells despite relatively unchanged levels of junctional proteins, we sought to uncover a mechanism connecting the a ATG9A to junctional dynamics. Recently, Atg9 was shown to be essential for normal development of the actin cytoskeleton in *Drosophila*

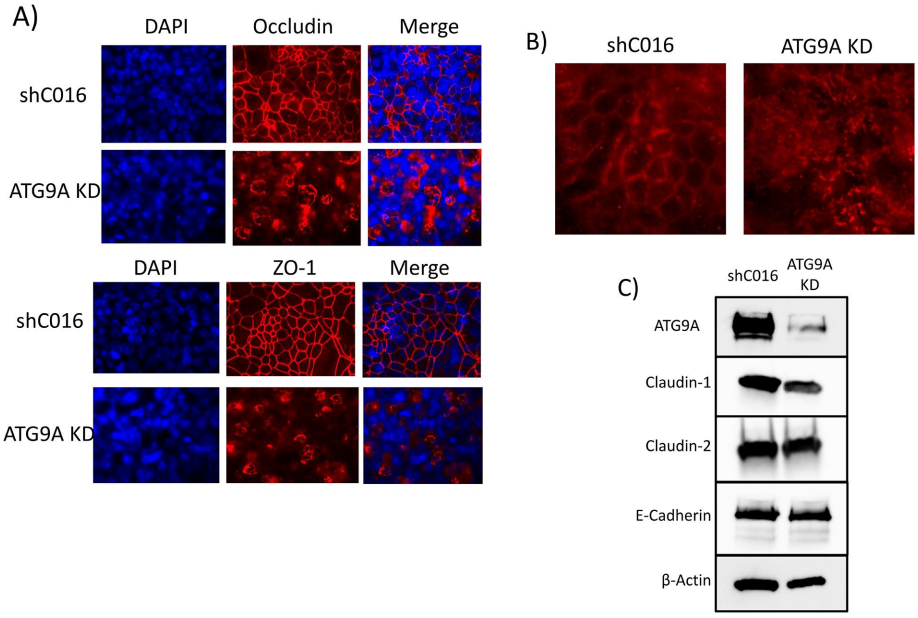

FIGURE 5: KD of ATG9A prevents proper TJ biogenesis. (A, B) T84-shC016 and T84 ATG9A KD cells were plated on transwell inserts, then fixed as described in *Materials and Methods* and stained for (A) ZO-1, occludin, or (B) E-cadherin. Representative images shown here. (C) Expression levels of junctional proteins were determined by western blot in whole cell lysates of either T84-shC016 or T84-shATG9A cells.

melanogaster (Kiss *et al.*, 2020). This study revealed that Atg9 interacts with the actin regulatory molecules profilin and Ena/VASP and that knockout of Atg9 resulted in distinct actin cytoskeleton defects. Further, the observed defects could not be recapitulated by disruption of other autophagy genes, suggesting a unique role for Atg9 distinct from its function in macroautophagy. The authors also observed that Ena/VASP was mislocalized and down-regulated in Atg9 knockout cells. Interestingly, we have shown in the past that the actin binding protein Ena/VASP is an essential component of TJ coupling to the cytoskeleton (Lawrence *et al.*, 2002). We therefore hypothesized that loss of ATG9A may compromise TJ formation through mislocalization of VASP and/or alterations to the actin cytoskeleton. To examine whether depletion of ATG9A affects the morphology of the actin cytoskeleton, monolayers of control and ATG9A cells were grown to confluence on transwell inserts and stained for β-actin and the TJ protein ZO-1, then observed by confocal microscopy. As shown in Figure 6A, β-actin staining in control cells appears similar to that seen in confluent T84 monolayers from previous publications (Ivanov *et al.*, 2005; Utech *et al.*, 2005). However, ATG9A-deficient cells demonstrate an abnormal actin cytoskeleton with numerous protuberances. These data suggest that actin polymerization in ATG9A-depleted cells may be dysfunctional as compared with control cells. To further examine this, we stained control and ATG9A-depleted cells for the actin regulatory protein VASP. Similar to previous observations, depletion of ATG9A resulted in mislocalization of VASP from the cell periphery. Control cells, by contrast, demonstrated distinct "halos" of VASP corresponding to ZO-1 localization. Taken together, these data suggest that loss of ATG9A imparts barrier defects in epithelial cells through pathologic alterations to the actin cytoskeleton and mislocalization of the essential TJ coupling factor VASP.

DISCUSSION

IBD is a multifactorial disease resulting from, among other factors, the interaction among the intestinal microbiome, the environment, and host genetics (Ananthakrishnan *et al.*, 2018). Although the etiology of IBD remains unclear, defects in autophagy have been implicated in predisposition to disease (Iida *et al.*, 2017). Previous studies have strongly implicated the HIF signaling pathway as a central component to establishment and maintenance of epithelial barrier, a crucial component of gut homeostasis (Ramakrishnan and Shah, 2016; Cummins and Crean, 2017). Here, we identified the autophagy protein ATG9A as a HIF target and as a novel barrier-regulatory factor in IECs. We demonstrate that ATG9A is positively regulated by hypoxia and HIF-1, and we further show that the absence of ATG9A is deleterious to epithelial barrier formation, suggesting that ATG9A plays a fundamental role in barrier formation and maintenance. Further, we demonstrate for the first time a novel role for ATG9A in the maintenance of the mammalian actin cytoskeleton.

The identification of ATG9A as a HIF/hypoxia-regulated protein is in agreement with previous findings that hypoxia orchestrates autophagic cellular responses, at least in part dependent on HIF (Zhang *et al.*, 2008; Bellot *et al.*, 2009; Hu *et al.*, 2012; Jawhari *et al.*, 2016). It is notable that in hypoxia, autophagy can be induced through at least three separate pathways, namely, the unfolded protein response (e.g., protein misfolding in the ER), AMPK activation as a result of energetic stress, and stabilization of HIF-α isoforms and subsequent induction of autophagy genes (Daskalaki *et al.*, 2018). The intent of this response is presumably to restore cellular homeostasis by normalizing energy levels and removing cellular insults. One such insult comes from mitochondria as, in hypoxic environments, they generate reactive oxygen species (ROS) at a much greater rate than at normoxia (Guzy *et al.*, 2005). In addition, the lack of molecular oxygen obviates the need for mitochondrial oxidative phosphorylation, as evidenced by the well-documented biochemical shift toward glycolysis in hypoxia (Agbor *et al.*, 2011). Thus, an adaptive arm of the hypoxic autophagy response is to control the number of mitochondria through "mitophagy," or mitochondrial-targeted autophagy (Liu *et al.*, 2012). ATG9A has been implicated in this process, as mouse embryonic fibroblasts lacking ATG9A could not recruit downstream autophagy proteins to mitochondria after mitotoxic stress (Itakura *et al.*, 2012). It is tempting to speculate that cells deficient in ATG9A would be unable to undergo mitophagy, even at normoxia, and would harbor an abundance of defective mitochondria. Such defective mitochondria have been shown to result in elevated ROS and altered cellular physiology, and defects in mitophagy have been linked to the pathogenesis of conditions as diverse as Parkinson's disease, cancer, and diabetic cardiomyopathy (Matsuda *et al.*, 2010; Palikaras *et al.*, 2018; Tong *et al.*, 2019; Vara-Perez *et al.*, 2019). Although polymorphisms in ATG9A have not been conclusively linked to IBD, it is possible that known defects (e.g., ATG16L1) could manifest dysfunctional ATG9A though pathway linkage. It is also entirely possible that disease-associated polymorphisms in *atg9a* exist, but have yet to be identified. Last, establishment of an epithelial barrier is exquisitely dependent on cellular energetics (Lee *et al.*, 2018). As autophagy is central to cellular energy homeostasis, it is possible that ATG9A KD cells

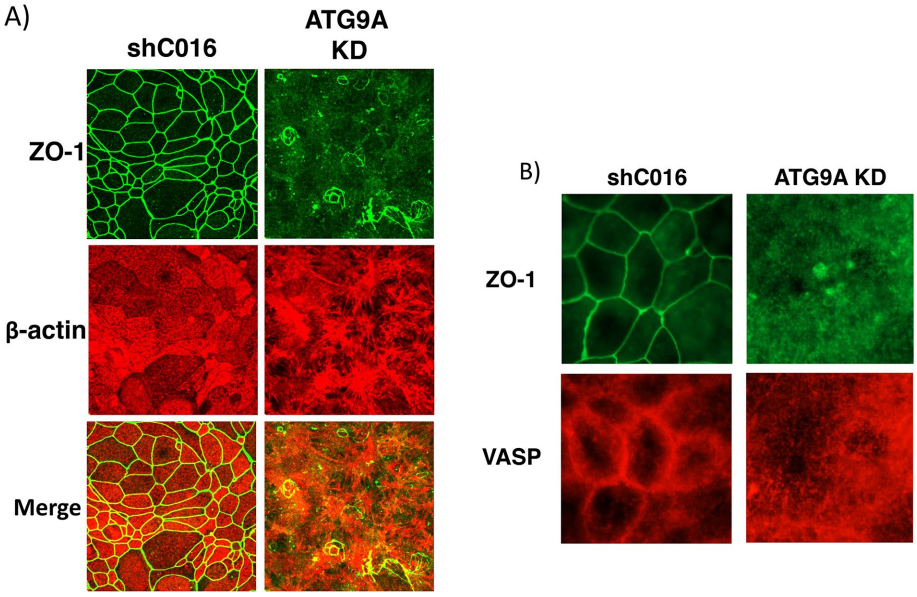

FIGURE 6: Depletion of ATG9A in T84 cells induces abnormalities in the actin cytoskeleton. (A) T84-shC016 or T84 ATG9A KD cells were plated on transwell inserts as described in *Materials and Methods* and costained for either ZO-1 and ACTB. (B) Costaining of either T84-shC016 or T84 ATG9A KD cells for ZO-1 and VASP.

simply lack the necessary energy capacity to establish barrier (Singh and Cuervo, 2011). Further experiments will seek to examine the energetic state of ATG9A-depleted cells, in the mode of previous studies that have probed the energetic state of intestinal epithelial monolayers (Lee *et al.*, 2018; Hall *et al.*, 2020; Lee *et al.*, 2020).

The role of autophagy as a biological process in maintenance of epithelial barrier function has been investigated, though mechanisms have not been well established. Previous studies have confirmed that potentiation of autophagy enhances barrier and, likewise, inhibition of autophagy weakens barrier (Nighot *et al.*, 2015; Wong *et al.*, 2019). Our results confirm these previous findings, as inhibition of autophagy by ATG9A KD or treatment with BafA1 was detrimental to epithelial barrier function. A dramatic observation in these studies was the magnitude of barrier dysfunction and mislocalization of TJ proteins in ATG9A KD cells. While these cells were grossly normal in appearance by phase contrast microscopy and proliferative capacity, barrier formation was decreased by more than 95% compared with controls. One possible way in which TJ homeostasis may depend on ATG9A is through the recycling of junctional molecules at the cell membrane. It has been shown, for example, that TJs are highly dynamic and undergo a continuous process of internalization through endosomal sorting to either recycle to the plasma membrane or target to late endosomes/lysosomes for degradation (Chalmers and Whitley, 2012; Stamatovic *et al.*, 2017). Further, this turnover can be modulated through external stimuli—a classic example is IFN-γ treatment of IECs, which induces internalization of TJ proteins into early/recycling endosomes through a ROCK- and myosin–II-dependent mechanism (Bruewer *et al.*, 2005; Utech *et al.*, 2005). IFN-γ plays an important role in the pathology of IBD, and previous studies have demonstrated the importance of this cytokine in intestinal inflammation (Colgan *et al.*, 1993, 1994). The precise role of ATG9A in the re-establishment of junctional complexes following inflammatory stimulus is an ongoing topic of research and may illuminate the process by which the epithelial barrier regenerates following insult.

The role of ATG9A in the maintenance of actin cytoskeletal integrity is noteworthy, as this is the first report in a mammalian system. Recently, Atg9 was shown to be essential for embryonic development of the actin cytoskeleton within *Drosophila* (Kiss *et al.*, 2020). Using both genetic and biochemical approaches, Atg9 was shown to interact directly with Ena-VASP. Indeed, using yeast two-hybrid approaches, it was shown that cytoplasmic domain 1 (CTD1, amino acids 1–117) of Atg9 directly interacts with Ena-VASP and that CTD4 binds to profilin. As we have previously shown that VASP coordinates TJ coupling to the actin cytoskeleton in both epithelia (Lawrence *et al.*, 2002) and endothelia (Comerford *et al.*, 2002), we examined VASP expression and localization in ATG9A-deficient cells. These experiments revealed a prominent mislocalization of VASP, implicating a role for ATG9A in VASP coupling to actin in mammalian cells. It is also notable that ATG9A has also been shown to interact with myosin II during macroautophagy, and the activity of myosin II is essential for autophagosome biogenesis (Tang *et al.*, 2011). Myosin Ic and VI have likewise been shown to be essential for macroautophagy (Tumbarello *et al.*, 2012; Brandstaetter *et al.*, 2014). It could be surmised, therefore, that ATG9A deficiency could significantly impact cellular functions that involve specific interactions with the cytoskelton, as was observed in *Drosophila* (Kiss *et al.*, 2020) and as we show here for barrier function. Although the full role that ATG9A plays in actin cytoskeletal dynamics remains to be elucidated, our work presents an interesting role for ATG9A in actin regulation and suggests future work to more fully characterize the role of ATG9A in actin dynamics. Moreover, it remains unclear whether this actin coupling to ATG9A is dependent or independent of autophagy. Additional work will be necessary to answer these questions.

In summary, the present observations provide a compelling argument for ATG9A as a fundamental component to barrier function in the mucosa. Additionally, they demonstrate a unique role for ATG9A in an autophagy-independent role in the regulation of the actin cytoskeleton and suggest that future targeting of ATG9A via novel therapeutics may be a viable strategy to reverse the barrier dysfunction commonly seen in intestinal inflammation.

MATERIALS AND METHODS

Cell culture

T84 cells (ATCC #CCL-248) were cultured in DMEM/F-12 1:1 (Thermo #11330032) containing Pen/Strep, GlutaMAX, and 10% (vol/vol) heat-inactivated bovine calf serum (BCS, Hyclone #SH30072.03). Caco-2 cells (ATCC #HTB-37) and HeLa cells (ATCC #CCL-2) were grown in IMDM (Corning #10-016-CV) containing Pen/Strep, GlutaMAX, and 10% BCS. C2BBe1 cells (ATCC #CRL-2102) were grown in EMEM (ATCC #30-2003) + 10% BCS. All cell lines were maintained at 37°C, 5% CO_2 in a humidified incubator. Preparation of polarized monolayers was accomplished by plating cells on 24-well transwell polyester inserts (Corning #3470). For hypoxia treatments, cells were incubated for the given period of time in a humidified, oxygen-controlled chamber (1% O_2, 5% CO_2, 94% N_2) using media that had been pre-equilibrated to reduce dissolved

Primer name	Sequence 5′→ 3′
actb_fwd (qPCR)	GCACTCTTCCAGCCTTCCTTCC
actb_rev (qPCR)	CAGGTCTTTGCGGATGTCCACG
atg9a_fwd (qPCR)	ACGAAGATGTGTTGGCTGTG
atg9a_rev (qPCR)	ATAAAGGACCTGCACACGGT
pASD1_F	CCCGGGTCGCTGTTCCTGAGGTAAGAtacaAGACCGGTTATTGGA
pASD1_R	TCCAATAACCGGTCTtgtaTCTTACCTCAGGAACAGCGACCCGGG
pASD2_F	CAGAGCCTCCCCAGGCGtacaGCTCACCAGGCTCAGGC
pASD2_R	GCCTGAGCCTGGTGAGCtgtaCGCCTGGGGAGGCTCTG

TABLE 1: Primers used.

oxygen content. Cells were passaged approximately every 7 d using either trypsin (Thermo #25200114) or TrypLE Express (Thermo #12604013). BafA1 (Calbiochem #508409) was used at a final concentration of 0.2 μM where indicated and 0.2% DMSO was used as a vehicle control for BafA1 experiments. Cells were treated 24 h after plating on transwell inserts. "Washouts" were performed by incubating the cells with the indicated treatment for 24 h, then immersing the inserts gently in sterile $HBSS^+$ (Hanks' balanced salt solution; Millipore-Sigma #H1387, supplemented with 10 mM HEPES, pH 7.4 [$HBSS^+$], sterile filtered at 0.22 μm) to remove the inhibitor and reincubating in fresh growth media.

Generation of KD cell lines

Generation of stable gene KD in T84 cells was performed through lentiviral delivery of shRNA. Briefly, lentiviral particles encoding shRNA against *atg9a* (TRCN0000244081), *hif1a* (TRCN0000003811), *hif2a/epas1* (TRCN0000003807), and *hif1b/arnt* (TRCN0000003817) were obtained from the Functional Genomics Facility (University of Colorado Anschutz; Aurora, CO; supported by Cancer Center Support Grant P30CA046934). shRNA sequences were previously designed by the RNAi Consortium (Broad Institute; Cambridge, MA). The nontargeting shRNA lentivirus shC016 was used as an experimental control. Infected cells were selected using puromycin and screened for KD efficiency by western blotting.

Chromatin immunoprecipitation ± DNA microarray (ChIP-chip)

ChIP-chip of hypoxia-treated Caco-2 cells has been described elsewhere (Glover *et al.*, 2013). In brief, Caco-2 cells were treated with hypoxia for 6 h, then fixed with 1% formaldehyde at 4°C for 10 min. Cell nuclei were then isolated and sonicated, with the resulting sheared DNA immunoprecipitated using either control IgG or rabbit polyclonal IgG against HIF-1α (Novus Biologicals #NB100-134) or HIF-2α (Novus Biologicals #NB100-122). Input DNA and HIF-1α/-2α-enriched samples were then amplified and hybridized to a custom human promoter (≤ 2 kB) microarray (Switchgear Genomics). Log_2-transformed ratios of HIF-1α/-2α-ChIP-Cy5 versus input-Cy3 were analyzed to assess genes differentially expressed in hypoxia, as well as genes that demonstrate an expression preference for either of the HIF-α isoforms. ChIP-chip data have previously been deposited on the NCBI Gene Expression Omnibus with the accession number GSE43108.

RNA isolation, cDNA synthesis, and qPCR analysis

RNA was isolated from T84 cells using TRIzol reagent (Thermo #15596018) according to the manufacturer's instructions. Isolated RNA was then reverse transcribed to cDNA using the iScript Supermix reagent (Bio-Rad #1708841), then analyzed using Power SYBR Green Master Mix reagent (Thermo #4367659) in an ABI 7300 Real-Time PCR System. Transcript quantities were calculated using an on-plate standard curve and normalized to β-actin. Primers used for real-time analysis are listed in Table 1. Statistical significance was calculated using *t* test (two-tailed, two-sample unequal variance).

SDS–PAGE and immunoblotting

Cell lysates were made by scraping cell monolayers in ice-cold RIPA buffer (50 mM Tris-HCl, 150 mM NaCl, 1% [vol/vol] IGEPAL CA-630, 0.5% [wt/vol] sodium deoxycholate, 0.1% [wt/vol] SDS, pH 8.0) containing 1× HALT Protease Inhibitor (Thermo #78429) and 5 mM EDTA, which were each added just prior to use. Lysates were normalized to total protein content using Pierce 660 nm Protein Reagent (Thermo #22660), and SDS–PAGE samples were made using 1× Sample Buffer (Bio-Rad #1610747) and freshly made 100 mM DTT. For analysis of ATG9A, samples were not boiled so as to prevent protein aggregation due to ATG9A's transmembrane nature. SDS–PAGE samples were run on Tris-glycine gels and transferred to 0.2 μm PVDF membranes using a Bio-Rad TransBlot Turbo system. Blots were blocked for 1 h at room temperature using blocking buffer–5% (wt/vol) milk (Bio-Rad #1706404) in Tris-buffered saline (TBS)-T (25 mM Tris-HCl, 150 mM NaCl, 0.1% [wt/vol] Tween-20), then incubated overnight in primary antibody diluted in blocking buffer. Primary antibodies used were anti-β-actin (Abcam #ab8227, 1/10000), anti-ATG9A (Abcam #ab108338, 1/1000), anti-BNIP3 (Abcam #ab109362, 1/1000), anti-BNIP3L (Abcam #ab109414, 1/1000), anti-Claudin-1 (Abcam #ab15098, 1/1000), anti-Claudin-2 (Abcam #ab53032, 1/1000), anti-E-cadherin (Abcam #ab40772, 1/10000), and anti-Occludin (Thermo #331500, 1/1000). Blots were then washed with TBS-T and incubated with HRP-conjugated secondary antibody diluted in blocking buffer (MP Biomedical #0855676, 0855550; 1/10000). After a second series of TBS-T washes, blots were developed using Clarity ECL reagent (Bio-Rad #1705060) and imaged using a Bio-Rad ChemiDoc MP.

Luciferase reporter assays

The LightSwitch reporter plasmid, in which the *atg9a* promoter region drives expression of an optimized Renilla luciferase, was ordered from Switchgear Genomics (Product #S707572) and verified by sequencing. HREs were identified in the *atg9a* promoter region of this plasmid using the web tool JASPAR (Fornes *et al.*, 2020). The ARNT::HIF-1α profile (MA0259.1) was used with an increased detection cut-off of 0.9, and only hits on the positive strand were considered. The location of the detected HREs, as well as their positions relative to the TSS, can be found in Figure 3A. Mutagenesis of these sites was performed using the QuikChange Lightning site-directed mutagenesis kit (Agilent #210518), with each of the core 5′-CGTG-3′ residues mutated to the opposite purine/pyrimidine.

The resulting mutation, 5′-TACA-3′, can be seen in context in Figure 3A. Primers used to conduct mutagenesis are described in Table 1 and were designed using the Agilent QuikChange web tool. The LightSwitch plasmid containing the *atg9a* promoter with two mutated HREs (pASD3) was verified by sequencing (Quintara Biosciences; Denver, CO). Plasmids were cloned into and maintained in *Escherichia coli* TOP10 (Thermo #C404003). Plasmid purification was done from cultures grown in LB-Miller broth + 100 µg/ml ampicillin using a HiSpeed Plasmid Midi Kit (Qiagen #12643). Both the WT and HRE-mutated plasmids were transfected into HeLa cells on 24-well plates at 5×10^4 cells/well using Fugene HD (Promega #E2311) according to the manufacturer's instructions; 24 h after transfection, cells were incubated either at normoxia or at hypoxia for 24 h using pre-equilibrated media. Normoxia/hypoxia-treated cells were then lysed and developed for luciferase activity (Promega #E1910). Luciferase activity levels were measured using a Promega GloMax 96-well system, with measurements in Figure 3B expressed as fold change of luciferase signal at hypoxia relative to normoxia for each construct.

Assessment of epithelial barrier function

T84-shC016 and T84-shATG9A cells were plated on 24-well transwell inserts, 0.4 µm pore size (Corning #3470). TEERs were monitored using an EVOM2 epithelial voltmeter (World Precision Instruments; Sarasota, FL). FITC-dextran permeability was determined by incubating cells in $HBSS^+$ containing 4 kDa FITC-dextran (Millipore-Sigma #FD4) in the upper "apical" compartment and monitoring diffusion of the tracer into the lower "basolateral" compartment at 37°C, in a manner described previously (Sanders *et al.*, 1995).

Immunofluorescence of polarized epithelial monolayers

Transwell-plated T84-shC016 and T84-shATG9A cells were fixed with cold (–20°C) methanol for 20 min at –20°C. Then, membranes were cut from transwell housing and placed into a fresh 24-well plate. Inserts were blocked for 1 h at room temperature in $HBSS^+$ containing 1% (wt/vol) bovine serum albumin (BSA; Millipore-Sigma #A4503). Then, inserts were stained with primary antibody diluted in $HBSS^+$/BSA for 1 h at room temperature. Primary antibodies used were anti-Occludin (Thermo #331500, 1/100), anti-ZO-1 (Thermo #339100 [mouse], 1/100; Thermo #617300 [rabbit], 1/50), anti-beta-actin (Abcam #ab8227, 1/1000), anti-VASP (BD #610448, 1/50), anti-E-Cadherin (Abcam #ab40772, 1/500), and anti-CD55 (Lawrence *et al.*, 2003) hybridoma supernatant (used undiluted). After a 5-min wash with $HBSS^+$/BSA, inserts were then stained with secondary antibody diluted in $HBSS^+$/BSA—either anti-rabbit (Thermo #A21206 [donkey], Alexa Fluor 488; Thermo #A11036 [goat], Alexa Fluor 568) or anti-mouse (Thermo #A11031 [goat], Alexa Fluor 568; Thermo #A21206 [donkey], Alexa Fluor 488). All secondary antibodies were used at 1/1000 dilution. Inserts were incubated in the dark for 1 h at room temperature with secondary antibody, then washed again with $HBSS^+$/BSA. Inserts were then placed onto glass slides and treated with a drop of ProLong Diamond + DAPI (Thermo #P36971). After 24 h curing time at room temperature in the dark, slides were imaged using a Zeiss Axio Imager A1 microscope. Slides were sealed with clear nail polish and stored long term in the dark at –20°C. Confocal analysis was performed using an Olympus FV1000 system confocal imaging system (Advanced Light Microscopy Core Facility; University of Colorado Anschutz, Aurora, CO).

Statistics and graphical presentation of data

Statistics and figure generation were performed using GraphPad Prism. Statistics were done using either *t* test or Mann–Whitney test, as indicated in the figure, with the *p* value specified if the results were significant ($p < 0.05$).

ACKNOWLEDGMENTS

This work was supported by National Institutes of Health grants DK1047893 (S.P.C.), DK50189 (S.P.C.), DK095491 (S.P.C.), and DK103639 (S.P.C.) and VA Merit BX002182 (S.P.C.).

REFERENCES

Abdul Rahim SA, Dirkse A, Oudin A, Schuster A, Bohler J, Barthelemy V, Muller A, Vallar L, Janji B, Golebiewska A, Niclou SP (2017). Regulation of hypoxia-induced autophagy in glioblastoma involves ATG9A. Br J Cancer 117, 813–825.

Abraham C, Cho JH (2009). Inflammatory bowel disease. N Engl J Med 361, 2066–2078.

Agbor TA, Cheong A, Comerford KM, Scholz CC, Bruning U, Clarke A, Cummins EP, Cagney G, Taylor CT (2011). Small ubiquitin-related modifier (SUMO)-1 promotes glycolysis in hypoxia. J Biol Chem 286, 4718–4726.

Allen EA, Baehrecke EH (2020). Autophagy in animal development. Cell Death Differ 27, 903–918.

Ananthakrishnan AN, Bernstein CN, Iliopoulos D, Macpherson A, Neurath MF, Ali RAR, Vavricka SR, Fiocchi C (2018). Environmental triggers in IBD: a review of progress and evidence. Nat Rev Gastroenterol Hepatol 15, 39–49.

Baumgart DC, Carding SR (2007). Inflammatory bowel disease: cause and immunobiology. Lancet 369, 1627–1640.

Bellot G, Garcia-Medina R, Gounon P, Chiche J, Roux D, Pouyssegur J, Mazure NM (2009). Hypoxia-induced autophagy is mediated through hypoxia-inducible factor induction of BNIP3 and BNIP3L via their BH3 domains. Mol Cell Biol 29, 2570–2581.

Brandstaetter H, Kishi-Itakura C, Tumbarello DA, Manstein DJ, Buss F (2014). Loss of functional MYO1C/myosin 1c, a motor protein involved in lipid raft trafficking, disrupts autophagosome-lysosome fusion. Autophagy 10, 2310–2323.

Bruewer M, Utech M, Ivanov AI, Hopkins AM, Parkos CA, Nusrat A (2005). Interferon-gamma induces internalization of epithelial tight junction proteins via a macropinocytosis-like process. FASEB J 19, 923–933.

Cartharius K, Frech K, Grote K, Klocke B, Haltmeier M, Klingenhoff A, Frisch M, Bayerlein M, Werner T (2005). MatInspector and beyond: promoter analysis based on transcription factor binding sites. Bioinformatics 21, 2933–2942.

Chalmers AD, Whitley P (2012). Continuous endocytic recycling of tight junction proteins: how and why? Essays Biochem 53, 41–54.

Chauhan S, Mandell MA, Deretic V (2015). IRGM governs the core autophagy machinery to conduct antimicrobial defense. Mol Cell 58, 507–521.

Colgan SP, Parkos CA, Delp C, Arnaout MA, Madara JL (1993). Neutrophil migration across cultured intestinal epithelial monolayers is modulated by epithelial exposure to IFN-gamma in a highly polarized fashion. J Cell Biol 120, 785–798.

Colgan SP, Parkos CA, Matthews JB, D'Andrea L, Awtrey CS, Lichtman AH, Delp-Archer C, Madara JL (1994). Interferon-gamma induces a cell surface phenotype switch on T84 intestinal epithelial cells. Am J Physiol 267, C402–C410.

Comerford KM, Lawrence DW, Synnestvedt K, Levi BP, Colgan SP (2002). Role of vasodilator-stimulated phosphoprotein in PKA-induced changes in endothelial junctional permeability. Faseb J 16, 583–585.

Cummins EP, Crean D (2017). Hypoxia and inflammatory bowel disease. Microbes Infect 19, 210–221.

Daskalaki I, Gkikas I, Tavernarakis N (2018). Hypoxia and selective autophagy in cancer development and therapy. Front Cell Dev Biol 6, 104.

Devriese S, Van den Bossche L, Van Welden S, Holvoet T, Pinheiro I, Hindryckx P, De Vos M, Laukens D (2017). T84 monolayers are superior to Caco-2 as a model system of colonocytes. Histochem Cell Biol 148, 85–93.

Fornes O, Castro-Mondragon JA, Khan A, van der Lee R, Zhang X, Richmond PA, Modi BP, Correard S, Gheorghe M, Baranasic D, *et al.* (2020). JASPAR 2020: update of the open-access database of transcription factor binding profiles. Nucleic Acids Res 48, D87–D92.

Furuta GT, Turner JR, Taylor CT, Hershberg RM, Comerford K, Narravula S, Podolsky DK, Colgan SP (2001). Hypoxia-inducible factor 1-dependent induction of intestinal trefoil factor protects barrier function during hypoxia. J Exp Med 193, 1027–1034.

Giatromanolaki A, Sivridis E, Maltezos E, Papazoglou D, Simopoulos C, Gatter KC, Harris AL, Koukourakis MI (2003). Hypoxia inducible factor 1alpha and 2alpha overexpression in inflammatory bowel disease. J Clin Pathol 56, 209–213.

Glover LE, Bowers BB, Saeedi B, Ehrentraut S, Kelly C, Burgess A, Campbell EL, Bayless A, Dobrinskikh E, Kendrick AA, *et al*. (2013). Control of creatine metabolism by HIF is an endogenous mechanism of barrier regulation in colitis. Proc Nat Acad Sci 110, 19820–19825.

Glover LE, Colgan SP (2017). Epithelial Barrier Regulation by Hypoxia-Inducible Factor. Ann Am Thorac Soc 14, S233–S236.

Guzy RD, Hoyos B, Robin E, Chen H, Liu L, Mansfield KD, Simon MC, Hammerling U, Schumacker PT (2005). Mitochondrial complex III is required for hypoxia-induced ROS production and cellular oxygen sensing. Cell Metab 1, 401–408.

Hall CHT, Lee JS, Murphy EM, Gerich ME, Dran R, Glover LE, Abdulla ZI, Skelton MR, Colgan SP (2020). Creatine transporter, reduced in colon tissues from patients with inflammatory bowel diseases, regulates energy balance in intestinal epithelial cells, epithelial integrity, and barrier function. Gastroenterology (*in press*).

Hartzell DD, Trinklein ND, Mendez J, Murphy N, Aldred SF, Wood K, Urh M (2009). A functional analysis of the CREB signaling pathway using HaloCHIP-chip and high throughput reporter assays. BMC Genomics 10, 497.

He G, Shankar RA, Chzhan M, Samouilov A, Kuppusamy P, Zweier JL (1999). Noninvasive measurement of anatomic structure and intraluminal oxygenation in the gastrointestinal tract of living mice with spatial and spectral EPR imaging. Proc Natl Acad Sci USA 96, 4586–4591.

Hu YL, DeLay M, Jahangiri A, Molinaro AM, Rose SD, Carbonell WS, Aghi MK (2012). Hypoxia-induced autophagy promotes tumor cell survival and adaptation to antiangiogenic treatment in glioblastoma. Cancer Res 72, 1773–1783.

Hu CJ, Wang LY, Chodosh LA, Keith B, Simon MC (2003). Differential roles of hypoxia-inducible factor 1alpha (HIF-1alpha) and HIF-2alpha in hypoxic gene regulation. Mol Cell Biol 23, 9361–9374.

Hugot JP, Chamaillard M, Zouali H, Lesage S, Cezard JP, Belaiche J, Almer S, Tysk C, O'Morain CA, Gassull M, *et al*. (2001). Association of NOD2 leucine-rich repeat variants with susceptibility to Crohn's disease. Nature 411, 599–603.

Iida T, Onodera K, Nakase H (2017). Role of autophagy in the pathogenesis of inflammatory bowel disease. World J Gastroenterol 23, 1944–1953.

Imai K, Hao F, Fujita N, Tsuji Y, Oe Y, Araki Y, Hamasaki M, Noda T, Yoshimori T (2016). Atg9A trafficking through the recycling endosomes is required for autophagosome formation. J Cell Sci 129, 3781–3791.

Itakura E, Kishi-Itakura C, Koyama-Honda I, Mizushima N (2012). Structures containing Atg9A and the ULK1 complex independently target depolarized mitochondria at initial stages of Parkin-mediated mitophagy. J Cell Sci 125, 1488–1499.

Ivanov AI, Hunt D, Utech M, Nusrat A, Parkos CA (2005). Differential roles for actin polymerization and a myosin II motor in assembly of the epithelial apical junctional complex. Mol Biol Cell 16, 2636–2650.

Jawhari S, Ratinaud MH, Verdier M (2016). Glioblastoma, hypoxia and autophagy: a survival-prone 'menage-a-trois'. Cell Death Dis 7, e2434.

Karhausen J, Furuta GT, Tomaszewski JE, Johnson RS, Colgan SP, Haase VH (2004). Epithelial hypoxia-inducible factor-1 is protective in murine experimental colitis. J Clin Invest 114, 1098–1106.

Kelly CJ, Glover LE, Campbell EL, Kominsky DJ, Ehrentraut SF, Bowers BE, Bayless AJ, Saeedi BJ, Colgan SP (2013). Fundamental role for HIF-1alpha in constitutive expression of human beta defensin-1. Mucosal Immunol 6, 1110–1118.

Kelly CJ, Zheng L, Campbell EL, Saeedi B, Scholz CC, Bayless AJ, Wilson KE, Glover LE, Kominsky DJ, Magnuson A, *et al*. (2015). Crosstalk between microbiota-derived short-chain fatty acids and intestinal epithelial HIF augments tissue barrier function. Cell Host Microbe 17, 662–671.

Kiss V, Jipa A, Varga K, Takáts S, Maruzs T, Lőrincz P, Simon-Vecsei Z, Szikora S, Földi I, Bajusz C, *et al*. (2020). Drosophila Atg9 regulates the actin cytoskeleton via interactions with profilin and Ena. Cell Death Differ 27, 1677–1692.

Lassen KG, Xavier RJ (2017). Genetic control of autophagy underlies pathogenesis of inflammatory bowel disease. Mucosal Immunol 10, 589–597.

Lawrence DW, Bruyninckx WJ, Louis NA, Lublin DM, Stahl GL, Parkos CA, Colgan SP (2003). Anti-adhesive role of apical decay-accelerating factor (DAF, CD55) in human neutrophil transmigration across mucosal epithelia. J Ex Med 198, 999–1010.

Lawrence DW, Comerford KM, Colgan SP (2002). Role of VASP in reestablishment of epithelial tight junction assembly after Ca2+ switch. Am J Physiol Cell Physiol 282, C1235–C1245.

Lee JS, Wang RX, Alexeev EE, Lanis JM, Battista KD, Glover LE, Colgan SP (2018). Hypoxanthine is a checkpoint stress metabolite in colonic epithelial energy modulation and barrier function. J Biol Chem 293, 6039–6051.

Lee JS, Wang RX, Goldberg MS, Clifford GP, Kao DJ, Colgan SP (2020). Microbiota-sourced purines support wound healing and mucus barrier function. iScience *In press*.

Lendahl U, Lee KL, Yang H, Poellinger L (2009). Generating specificity and diversity in the transcriptional response to hypoxia. Nat Rev Genet 10, 821–832.

Liu L, Feng D, Chen G, Chen M, Zheng Q, Song P, Ma Q, Zhu C, Wang R, Qi W, *et al*. (2012). Mitochondrial outer-membrane protein FUNDC1 mediates hypoxia-induced mitophagy in mammalian cells. Nat Cell Biol 14, 177–185.

Louis NA, Hamilton KE, Canny G, Shekels LL, Ho SB, Colgan SP (2006). Selective induction of mucin-3 by hypoxia in intestinal epithelia. J Cell Biochem 99, 1616–1627.

Massey DC, Bredin F, Parkes M (2008). Use of sirolimus (rapamycin) to treat refractory Crohn's disease. Gut 57, 1294–1296.

Matsuda N, Sato S, Shiba K, Okatsu K, Saisho K, Gautier CA, Sou YS, Saiki S, Kawajiri S, Sato F, *et al*. (2010). PINK1 stabilized by mitochondrial depolarization recruits Parkin to damaged mitochondria and activates latent Parkin for mitophagy. J Cell Biol 189, 211–221.

Menikdiwela KR, Ramalingam L, Rasha F, Wang S, Dufour JM, Kalupahana NS, Sunahara KKS, Martins JO, Moustaid-Moussa N (2020). Autophagy in metabolic syndrome: breaking the wheel by targeting the renin-angiotensin system. Cell Death Dis 11, 87.

Mi H, Muruganujan A, Ebert D, Huang X, Thomas PD (2019). PANTHER version 14: more genomes, a new PANTHER GO-slim and improvements in enrichment analysis tools. Nucleic Acids Res 47, D419–D426.

Mutalib M, Borrelli O, Blackstock S, Kiparissi F, Elawad M, Shah N, Lindley K (2014). The use of sirolimus (rapamycin) in the management of refractory inflammatory bowel disease in children. J Crohns Colitis 8, 1730–1734.

Nighot PK, Hu CA, Ma TY (2015). Autophagy enhances intestinal epithelial tight junction barrier function by targeting claudin-2 protein degradation. J Biol Chem 290, 7234–7246.

Ogura Y, Bonen DK, Inohara N, Nicolae DL, Chen FF, Ramos R, Britton H, Moran T, Karaliuskas R, Duerr RH, *et al*. (2001). A frameshift mutation in NOD2 associated with susceptibility to Crohn's disease. Nature 411, 603–606.

Palikaras K, Lionaki E, Tavernarakis N (2018). Mechanisms of mitophagy in cellular homeostasis, physiology and pathology. Nat Cell Biol 20, 1013–1022.

Ramakrishnan SK, Shah YM (2016). Role of intestinal HIF-2alpha in health and disease. Annu Rev Physiol 78, 301–325.

Saeedi BJ, Kao DJ, Kitzenberg DA, Dobrinskikh E, Schwisow KD, Masterson JC, Kendrick AA, Kelly CJ, Bayless AJ, Kominsky DJ, *et al*. (2015). HIF-dependent regulation of claudin-1 is central to intestinal epithelial tight junction integrity. Mol Biol Cell 26, 2252–2262.

Saitoh T, Fujita N, Hayashi T, Takahara K, Satoh T, Lee H, Matsunaga K, Kageyama S, Omori H, Noda T, *et al*. (2009). Atg9a controls dsDNA-driven dynamic translocation of STING and the innate immune response. Proc Natl Acad Sci USA 106, 20842–20846.

Sanders SE, Madara JL, McGuirk DK, Gelman DS, Colgan SP (1995). Assessment of inflammatory events in epithelial permeability: a rapid screening method using fluorescein dextrans. Epithelial Cell Biol 4, 25–34.

Schodel J, Oikonomopoulos S, Ragoussis J, Pugh CW, Ratcliffe PJ, Mole DR (2011). High-resolution genome-wide mapping of HIF-binding sites by ChIP-seq. Blood 117, e207–e217.

Singh R, Cuervo AM (2011). Autophagy in the cellular energetic balance. Cell Metab 13, 495–504.

Stamatovic SM, Johnson AM, Sladojevic N, Keep RF, Andjelkovic AV (2017). Endocytosis of tight junction proteins and the regulation of degradation and recycling. Ann N Y Acad Sci 1397, 54–65.

Tang HW, Wang YB, Wang SL, Wu MH, Lin SY, Chen GC (2011). Atg1-mediated myosin II activation regulates autophagosome formation during starvation-induced autophagy. EMBO J 30, 636–651.

Taylor CT, Colgan SP (2017). Regulation of immunity and inflammation by hypoxia in immunological niches. Nat Rev Immunol 17, 774–785.

Tong M, Saito T, Zhai P, Oka SI, Mizushima W, Nakamura M, Ikeda S, Shirakabe A, Sadoshima J (2019). Mitophagy is essential for maintaining cardiac function during high fat diet-induced diabetic cardiomyopathy. Circ Res 124, 1360–1371.

Tumbarello DA, Waxse BJ, Arden SD, Bright NA, Kendrick-Jones J, Buss F (2012). Autophagy receptors link myosin VI to autophagosomes to

mediate Tom1-dependent autophagosome maturation and fusion with the lysosome. Nat Cell Biol 14, 1024–1035.
Utech M, Ivanov AI, Samarin SN, Bruewer M, Turner JR, Mrsny RJ, Parkos CA, Nusrat A (2005). Mechanism of IFN-gamma-induced endocytosis of tight junction proteins: myosin II-dependent vacuolarization of the apical plasma membrane. Mol Biol Cell 16, 5040–5052.
Vara-Perez M, Felipe-Abrio B, Agostinis P (2019). Mitophagy in cancer: a tale of adaptation. Cells 8.
Walfish AE, Ching Companioni RA. (April 2019). Drugs for inflammatory bowel disease. In: Merck Manual, Kenilworth, NJ: Merck and Co.
Wang D, Naydenov NG, Feygin A, Baranwal S, Kuemmerle JF, Ivanov AI (2016). Actin-depolymerizing factor and cofilin-1 have unique and overlapping functions in regulating intestinal epithelial junctions and mucosal inflammation. Am J Pathol 186, 844–858.
Wang RX, Lee JS, Campbell EL, Colgan SP (2020). Microbiota-derived butyrate dynamically regulates intestinal homeostasis through regulation of the actin-associated protein synaptopodin. Proc Nat Acad Sci 117, 11648–11657.
Wartenberg M, Ling FC, Muschen M, Klein F, Acker H, Gassmann M, Petrat K, Putz V, Hescheler J, Sauer H (2003). Regulation of the multidrug resistance transporter P-glycoprotein in multicellular tumor spheroids by hypoxia-inducible factor (HIF-1) and reactive oxygen species. Faseb J 17, 503–505.
Weerasekara VK, Panek DJ, Broadbent DG, Mortenson JB, Mathis AD, Logan GN, Prince JT, Thomson DM, Thompson JW, Andersen JL (2014). Metabolic-stress-induced rearrangement of the 14–3-3ζ interactome promotes autophagy via a ULK1- and AMPK-regulated 14–3-3ζ interaction with phosphorylated Atg9. Mol Cell Biol 34, 4379–4388.
Wong M, Ganapathy AS, Suchanec E, Laidler L, Ma T, Nighot P (2019). Intestinal epithelial tight junction barrier regulation by autophagy-related protein ATG6/beclin 1. Am J Physiol Cell Physiol 316, C753–C765.
Yamada T, Carson AR, Caniggia I, Umebayashi K, Yoshimori T, Nakabayashi K, Scherer SW (2005). Endothelial nitric-oxide synthase antisense (NOS3AS) gene encodes an autophagy-related protein (APG9-like2) highly expressed in trophoblast. J Biol Chem 280, 18283–18290.
Yamamoto S, Ma X (2009). Role of Nod2 in the development of Crohn's disease. Microbes Infect 11, 912–918.
Zhang H, Bosch-Marce M, Shimoda LA, Tan YS, Baek JH, Wesley JB, Gonzalez FJ, Semenza GL (2008). Mitochondrial autophagy is an HIF-1-dependent adaptive metabolic response to hypoxia. J Biol Chem 283, 10892–10903.
Zheng L, Kelly CJ, Battista KD, Schaefer R, Lanis JM, Alexeev EE, Wang RX, Onyiah JC, Kominsky DJ, Colgan SP (2017). Microbial-derived butyrate promotes epithelial barrier function through IL-10 receptor-dependent repression of Claudin-2. J Immunol 199, 2976–2984.